Colloid Polym Sci 274:245–252 (1996)

ORIGINAL CONTRIBUTION

H. Hirata
S. Katayama
H. Okabayashi
M. Furusaka
T. Kawakatsu

A small-angle neutron scattering study of the ethyl (*n*-octyl) phosphate micelles in water

Received: 14 July 1995
Accepted: 31 August 1995

H. Hirata · S. Katayama
Dr. H. Okabayashi (✉)
Department of Applied Chemistry
Nagoya Institute of Technology
Gokiso-cho, Showa-ku
Nagoya 466, Japan

M. Furusaka
BSF, National Laboratory
for High Energy Physics
1-1 Oho, Tsukuba-shi
Ibaraki 305, Japan

T. Kawakatsu
Department of Physics
Tokyo Metropolitan University
Hachioji, Tokyo 192-03, Japan

Summary Mixed-double chain anionic surfactants, barium- and lithium-salts of ethyl(*n*-octyl) phosphate (EOP), which are asymmetric in the molecular shape, and a series of identical chain di-*n*-alkyl phosphate lithium salts have been synthesized. The limiting partial molar volume of a PO_4^- group (23.43 ± 0.41 cm^3 mol^{-1}) for use in small-angle neutron scattering analysis was determined by density measurements of a series of identical chain di-*n*-alkyl phosphate lithium salts. For lithium EOP-D_2O system, a critical micellar concentration (2.3 wt%) was determined by ^{31}P NMR spectra. The micellar shape and size in the EOP-water binary system has been investigated by using small-angle neutron scattering (SANS) spectra. It has been found that the micelles of barium EOP in water have the shape of a prolate spheroid and aggregation numbers (**n**) equal to 48 at 23° C and 52 at 50° C. For the lithium EOP-micellar system, it has been found that the minimum micelle with an aggregation number $\mathbf{n} = 21$ is spherical and micellar growth and variation from the spherical to the prolate shape might occur with an increase in concentration above the CMC.

Key words Ethyl(*n*-octyl) phosphate – micelle – SANS

Introduction

The type and structure of an aggregate formed by different surfactant molecules depend on their geometrical packing properties [1], which can be represented by the characteristic packing parameters of a given surfactant molecule. For surfactant molecules of optimal area $\mathbf{a}_0$, hydrocarbon volume **v** and critical chain length $\mathbf{l}_c$, Israelachvili et al. [1] have shown that the value of the packing parameter ($\mathbf{v}/\mathbf{a}_0\mathbf{l}_c$) determines the shape of an aggregate. A packing property can be easily changed by many factors such as ionic environment, temperature, polar-group size, length and unsaturation of a hydrocarbon chain [2–7]. Therefore, in order to discuss the quantitative details of the relationship between the geometrical packing property of a surfactant molecule and factors affecting the aggregate structure, further systematic studies on the molecular design and synthesis of a surfactant molecule and the aggregate structure are essential.

We have synthesized the lithium salts of ethyl(*n*-octyl) phosphate, *n*-propyl(*n*-heptyl) phosphate and *n*-butyl(*n*-hexyl) phosphate, and the phage diagrams and phase structures of these double chain surfactant-water systems have been determined [8]. These mixed double-chain anionic surfactants have different packing parameters characteristic of each molecule. The problem of the relationship between the geometrical packing properties and factors such as the structure of an aggregate formed by these surfactants in water remains as a challenge to our interest.

Colloid & Polymer Science, Vol. 274, No. 3 (1996)

Recently, for the barium-salts of ethyl(*n*-octyl) phosphate (EOP) in water, the phase diagram and phase structure has been determined [9, 10]. In particular, self-diffusion coefficient vs. inverse concentration plots could be explained by a simple two-site model and a single monomer⇔micelle equilibrium [11, 12], and provided the CMC value which was in good agreement with that determined by ^{31}P NMR chemical shift vs. inverse concentration plots [9]. The x-ray low-angle diffraction data have supported the evidence for the structural change in the aggregate system at low water-content, which has been assumed from the self-diffusion behaviour [10]. Moreover, the conformation of EOP anions in EOP-water system has been investigated by ^{13}C NMR, infrared and Raman spectroscopic methods [9, 13]. However, shape and size of an EOP micelle remains unresolved.

EOP anion

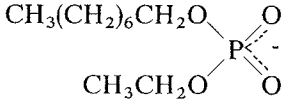

Techniques available for structural determination of micellar shape and size in aqueous solutions include quasi-elastic light scattering, small-angle x-ray scattering (SAXS) and small-angle neutron scattering (SANS). Of these, SANS can provide not only size information but more detailed structural information on individual regions of the aggregate. Therefore, SANS has been used successfully to determine the structure of anionic and cationic surfactant micelles [14–17].

In the present paper, the aggregate structures formed by barium- and lithium-salts of EOP in water are discussed in detail, using SANS and their analyses.

Experimental

Materials

Barium Ba(EOP) and lithium Li(EOP) salts of ethyl(*n*-octyl) phosphate (EOP) were prepared as follows. Ethylphosphorodichloridate ($C_2H_5OP(O)Cl_2$, b.p. 65 ~ 67° C at 25 mmHg), prepared using phosphoryl chloride and ethylalcohol and vacuum-distilled, was converted to ethyl(*n*-octyl) phosphorochloridate ($(C_2H_5O)(C_8H_{17}O)P(O)Cl$) [18]. The $(C_2H_5O)(C_8H_{17}O)P(O)Cl$ sample was vacuum-distilled several times (b.p. 121 ~ 123° C at 4 mmHg) and was treated with benzaldoxim (Furuka Chemie AG) by the method of Mukaiyama et al. [19], to yield phosphoric acid ethyl(*n*-octyl)ester, $(C_2H_5O)(C_8H_{17}O)P(O)OH$. Phosphoric acid ethyl(*n*-octyl)ester was then neutralized with aqueous solutions of barium or lithium hydroxide. Products were analyzed by ^{1}H and ^{13}C NMR and by elemental analysis. Anal. $C_{20}H_{44}O_8P_2Ba$: Calcd: C, 39.26; H, 7.25; Found: C, 39.12; H, 7.29, $C_{10}H_{22}PO_4Li$: Calcd: C, 49.18; H, 9.08; Found: C, 48.86; H, 9.25.

A series of identical chain di-*n*-alkyl phosphate lithium salts ($((CH_3(CH_2)_nO)_2PO_2^-Li^+$, $n = 0, 1, 2, 3, 4$ and 5; $Li^+(R\text{-}O)_2PO_2^-$) was similarly prepared using phosphoryl-chloride and the corresponding *n*-alcohols by the same procedures. The identification of these products was also established by ^{1}H and ^{13}C NMR spectra and elemental analysis. The agreement between the calculated and observed values of elemental analysis was within 0.5%.

The solvents were D_2O (Wako Pure Chemical Industries, LTD) 99.8 atom % of deuterium and a deionized and twice-distilled H_2O.

Molal volume determination

The apparent molal volumes (Φ_{app}) of a series of identical chain di-*n*-alkyl phosphate lithium salts were calculated from the densities of the sample-H_2O and -D_2O solutions, measured with an Anton Paar vibrating tube digital densitometer Model DMA 602/60 at 298.15 ± 0.01 K. The thermal stability of the liquid flowing through the jacket around the density measuring cell was maintained within ±0.01 K by a temperature controller. The densitometer was calibrated with the known densities of air and water. Reproducibility of the density measurements was better than 3 ppm. The apparent molar volume Φ_{app} may then be calculated from the density (d, g cm^{-3}) of the solution using:

$$\Phi_{app} = \frac{1}{m}\left[\frac{1000 - mM}{d} - \frac{1000}{d_s}\right], \quad (1)$$

where m is the molarity, d_s the density of the solvent and M the molar weight of the solute.

^{31}P NMR measurements

^{31}P NMR spectra were measured using high-power proton decoupling at 80.995 MHz on a Varian XL-200 spectrometer. The ^{31}P chemical shifts (σ) of the EOP anions in D_2O solution were measured relative to the ^{31}P signal of aqueous 85%-H_3PO_4 solution as an external reference.

Neutron scattering measurements

The small-angle neutron scattering (SANS) measurements were carried out by small- and medium-angle neutron

scattering instruments (SAN and WINK) installed at the pulsed neutron source KENS at National Laboratory for High Energy Physics, Tsukuba, Japan [20, 21]. The sample solutions were placed in a quartz cell of 1 or 2 mm path length. The scattering length density (ρ) of each component was calculated using the following equation,

$$\rho = \Sigma\, b_i/V\,, \tag{2}$$

where b_i is the scattering length of atom i and V is the molecular volume. The scattering length densities used for the SANS data analysis were quoted from ref. [22]. The magnitude of the momentum transfer (Q) is given by:

$$Q = \frac{4\pi}{\lambda}\sin\left(\frac{\theta}{2}\right), \tag{3}$$

where λ is the incident wavelength (3 ~ 11 Å for SAN and 1 ~ 16 Å for WINK) and θ the scattering angle. The intensity of scattered neutrons was recorded on a position-sensitive 2-D detector. Scattering intensity from the sample solutions were corrected for detector background and sensitivity, empty cell scattering, incoherent scattering, and sample transmission. Solvent intensity was subtracted from that of sample. The resulting corrected intensities were converted to radial averages versus Q using programs provided by the KENS. Normalization of the data to an absolute intensity scale was made by using the transmission of a 1 mm water sample. Corrections for multiple scattering were also made [23].

The SANS measurements were made at three different temperatures (23°, 40°, 50° C) for the Ba(EOP) samples and at 23° C for the Li(EOP) samples. Thermal stability was maintained within ±0.1° C.

SANS analysis

The dependence of the neutron scattering intensity $d\Sigma(Q)/d\Omega$ on the magnitude of a scattering vector (Q) can be expressed as a function of both the particle structure factor $P(Q)$ and the interparticle structure factor $S'(Q)$ as follows,

$$\frac{d\Sigma(Q)}{d\Omega} = I_0 P(Q) S'(Q)\,. \tag{4}$$

When the interaction between micelles is neglected, the interparticle structure factor is reduced to unity ($S'(Q) = 1$). In the small-angle scattering region, the terms in Eq. (4) can be written in the Guinier approximation [24] by the following form.

$$\ln\frac{d\Sigma(Q)}{d\Omega} = \ln I_0 - \frac{R_g^2}{3}Q^2\,, \tag{5}$$

where R_g is the radius of gyration of the particle. The R_g value can be given in terms of the geometrical parameters for a particle. For the prolate ellipsoid particle consisting of double layers, R_g is given by the following form [25].

$$R_g^2 = \frac{W_1 R_{g1}^2 + W_2 R_{g2}^2}{W_1 + W_2} \tag{6}$$

$$R_{g1}^2 = \frac{\mathbf{a}^2 + 2\mathbf{b}^2}{5} \tag{7}$$

$$R_{g2}^2 = \frac{[(\mathbf{a}+\mathbf{t})^2 + 2(\mathbf{b}+\mathbf{t})^2]\,(\mathbf{a}+\mathbf{t})(\mathbf{b}+\mathbf{t})^2 - (\mathbf{a}^2 + 2\mathbf{b}^2)\mathbf{a}\mathbf{b}^2}{5[(\mathbf{a}+\mathbf{t})(\mathbf{b}+\mathbf{t})^2 - \mathbf{a}\mathbf{b}^2]}\,, \tag{8}$$

where weighing factor W_1 and W_2 are $W_1 = (\rho_s - \rho_c)V_c$ and $W_2 = (\rho_s - \rho_p)V_p$, respectively. **a** Å and **b** Å are micellar axes, **t** Å the diameter (4.2 Å) of polar head groups (PO_4^-). V_c Å^3, V_p Å^3 and V_m ($= V_c + V_p$) Å^3 are the volumes of the micelle core, the polar shell and overall micelle, respectively. ρ_c Å^{-2}, ρ_p Å^{-2} and ρ_s Å^{-2} are the average neutron scattering length densities of the hydrophobic core, polar shell and solvent, respectively.

The particle structure factor is expressed by the following form,

$$P(Q) = \int_0^1 |F(Q,\mu)|^2\, d\mu \tag{9}$$

$$F(Q,\mu) = x\left(\frac{3(\sin(QR_1) - QR_1\cos(QR_1))}{(QR_1)^3}\right) + (1-x)\left(\frac{3(\sin(QR_2) - QR_2\cos(QR_2))}{(QR_2)^3}\right), \tag{10}$$

$$x = \frac{(\rho_p - \rho_c)V_c}{(\rho_p - \rho_c)V_c + (\rho_s - \rho_p)V_m} \tag{11}$$

where μ is the cosine of the angle between the scattering vector Q and the micellar axis **b**.

When the micellar shape is prolate, R_1 and R_2 are given by

$$R_1 = [\mathbf{a}^2\mu^2 + \mathbf{b}^2(1-\mu^2)]^{1/2} \tag{12}$$

$$R_2 = [(\mathbf{a}+\mathbf{t})^2\mu^2 + (\mathbf{b}+\mathbf{t})^2(1-\mu^2)]^{1/2}\,. \tag{13}$$

For micellar solution systems having interparticle interactions, the interaction peak appears in the SANS intensity spectrum. Therefore, in order to interpret the SANS data, it is necessary to calculate I_0, $P(Q)$ and $S'(Q)$ on the basis of a micellar model. I_0 is given by the following form,

$$I_0 = \frac{(C - \mathrm{CMC})N_A}{1000\,n}10^{-16}[(\rho_p - \rho_c)V_c + (\rho_s - \rho_p)V_m]^2\,. \tag{14}$$

Colloid & Polymer Science, Vol. 274, No. 3 (1996)

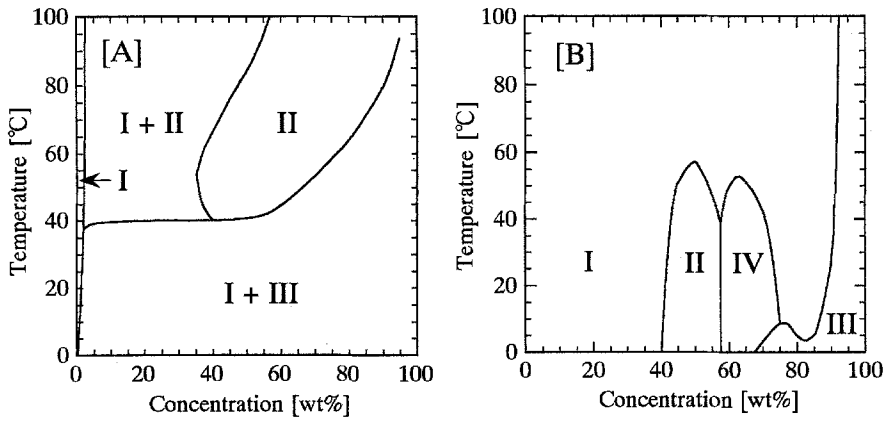

Fig. 1 Phase diagram of the Ba(EOP)-H_2O [A] and Li(EOP)-H_2O [B] systems. region I: homogeneous transparent solution (monomer⇔micelle equilibrium solution); region II: lyotropic liquid crystalline phase; region III: coagel phase; region IV: transparent hard gel phase

The interparticle structure factor $S'(Q)$ can be calculated for using the rescaled means spherical approximation given by Hayter et al. [26–28].

Results and discussion

Phase diagrams of Ba(EOP) and Li(EOP) systems

A phase diagram of the binary Ba(EOP)-water system consists of four regions [9], as shown in Fig. 1 [A].

Region I is a homogeneous aqueous solution, in which the EOP anions are in the monomeric state below 1.2 wt% (0.029 M), the critical micelle concentration (CMC) [9]. In particular, it should be noted that the monomer⇔micelle equilibrium region is very narrow and the micellar concentration is very small. Region II is a lyotropic liquid crystalline phase. It has been deduced from the x-ray diffraction study [10] that the lamellar-like aggregate is preferentially stabilized in this region and that its structure strongly depends on the concentration.

The phase diagram of the Li(EOP)-water system consists of four regions [8], as shown in Fig. 1 [B]. In the present study, the aggregate structures in region I which is a homogeneous aqueous solution, have been investigated by SANS analysis.

Only narrow and symmetrical ^{31}P resonance signals were observed for region I, reflecting an isotropic motional averaging of monomers and Brownian tumbling of the EOP micelles. The ^{31}P chemical shift (σ) vs. inverse concentration ($1/C$) plot for Li(EOP)-D_2O system is shown in Fig. 2. The inflection point is observed at concentration 2.3 wt%. Such a concentration dependence of the ^{31}P σ values can also be explained by a pseudo-phase and two-site model [11, 12]. The observed chemical shift (σ) is a weighted average of the chemical shifts in the monomeric and in the micellar state, since the exchange rate of the EOP anions between the bulk solution and the micelles is

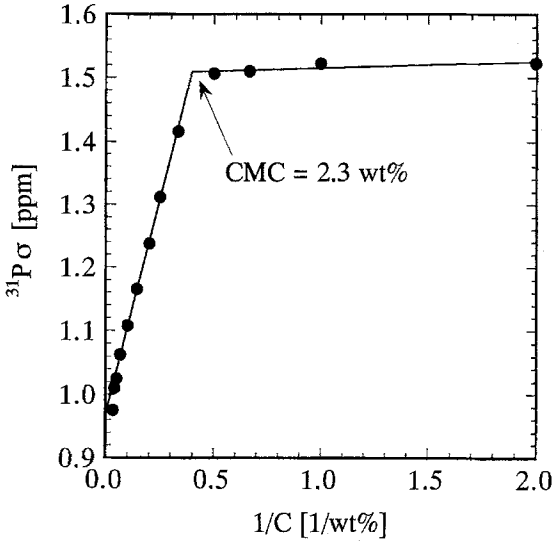

Fig. 2 ^{31}P chemical shift (σ) vs. 1/C plots for Li(EOP)-D_2O system region I

generally fast on the NMR time scale. Thus, the observed σ value is expressed [29] by:

$$\sigma = (\mathrm{CMC}/C)\,\sigma_{\mathrm{mono}} + [(C - \mathrm{CMC})/C]\,\sigma_{\mathrm{mic}} \qquad (15)$$

(assuming that the concentration in the monomeric state is constant above the CMC), where C is the total concentration of EOP, and σ_{mono} and σ_{mic} are the ^{31}P chemical shifts for the monomers and micelles, respectively. Plots of σ vs. $1/C$ are well described by Eq. (15).

In order to determine the limiting partial molal volume (Φ^0) of a PO_4^- group, the apparent molal volumes (Φ_{app}) for a series of identical chain di-*n*-alkylphosphate lithium salts ($Li^+(R\text{-}O)_2PO_2^-$) were determined at 298.15 K from density measurements. Figure 3A shows concentration dependence of Φ_{app} for a series of di-*n*-alkylphosphate lithium salts in H_2O with increased chain length. The

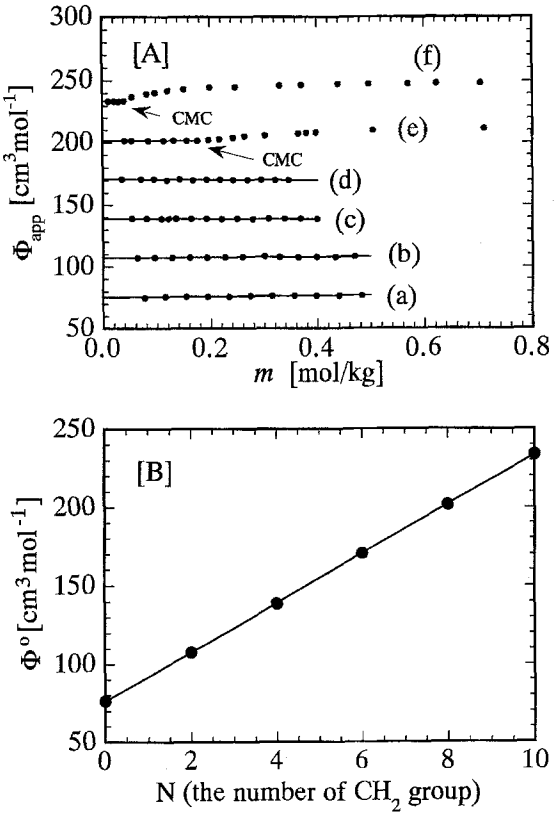

Fig. 3A Concentration dependence of Φ_{app} for a series of identical chain di-*n*-alkyl phosphate lithium salts-H_2O solutions. (a) di-methyl-phosphate, (b) di-ethyl phosphate, (c) di-*n*-propyl phosphate, (d) di-*n*-butylphosphate, (e) di-*n*-pentyl phosphate and (f) di-*n*-hexyl phosphate. **B** The CH_2 number dependence of the Φ^0 value for a series of identical chain di-*n*-alkyl phosphate lithium salts

Φ^0 values for these solutes in water were evaluated from the apparent molal volumes by means of Eq. (1).

As shown in Fig. 3B, the CH_2-number dependence of the Φ^0 value for a series of samples in water provided a linear relationship ($\Phi^0 = 76.22 + 15.71$ N) between the Φ^0 value and the CH_2-number (N). The Φ^0 value 15.71 ± 0.30 cm^3 mol^{-1} for the CH_2 group was evaluated from the slope and is very close to the $\Phi^0(CH_2)$ value which has already been reported [30]. Extrapolation to the intercept provides summation ($\Phi^0_{sum} = \Phi^0(PO_4^-) + \Phi^0(Li^+) + 2\Phi^0(H)$) of the Φ^0 value of a PO_4^- group, a Li^+ ion and that of two protons belonging to the terminal CH_3 groups. The Φ^0 value of the PO_4^- group can be calculated from the observed $\Phi^0(CH_2)$ and Φ^0_{sum} values, the known $\Phi^0(CH_3)$ values and $\Phi^0(Li^+)$ value [31], using the additive rule. Thus, in the present study, the Φ^0 values 23.43 ± 0.41 cm^3 mol^{-1} for a PO_4^- group was obtained and is used for the SANS analysis.

In order to estimate the isotope effect on the Φ^0 value of a PO_4^- group, density measurements were also made for the di-*n*-pentyl phosphate-D_2O solutions. The isotope effect was found to be about 0.3%. Thus, the Φ^0 value of a PO_4^- group, obtained for a series of identical chain di-*n*-alkylphosphate lithium salts in H_2O, was used for a SANS analysis.

Micellar structure of Ba(EOP)

In the present study, emphasis is given to discussion of the phase structures in region I, as a result of the SANS analysis.

For region I, two sample solutions, 1.0 wt% (below the CMC) and 2.0 wt% (above the CMC), were used for the SANS measurements. At concentrations above 2.0 wt%, a phase separation occurs and region II newly appears. Therefore, for the sample solution in region I, the 2.0 wt% concentration is close to the maximum concentration, for which SANS measurements are possible.

Figure 4A shows the data of $I(Q)$ against Q observed at concentrations of 1.0 and 2.0 wt% for the Ba(EOP)-D_2O

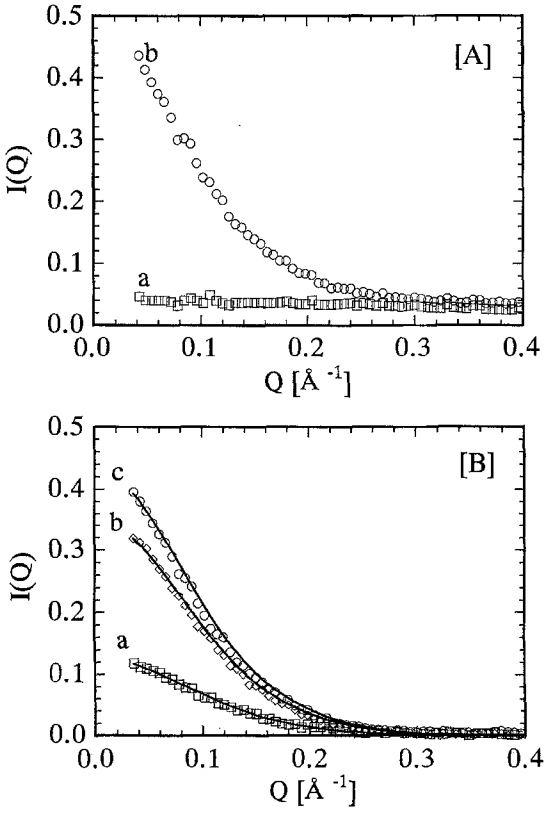

Fig. 4A SANS spectra of the Ba(EOP)-D_2O solutions (a: 1.0 wt% and b: 2.0 wt% at 50° C). **B** Temperature dependence (a: 23° C, b: 40° C, c: 50°C) of the scattered intensity for the 2.0 wt% sample, in which the scattered intensities of the 1.0 wt% solution were subtracted from the observed intensities, and fitted scattering intensity profiles (solid lines) in the Q range 0.03 ~ 0.40 [Å^{-1}]

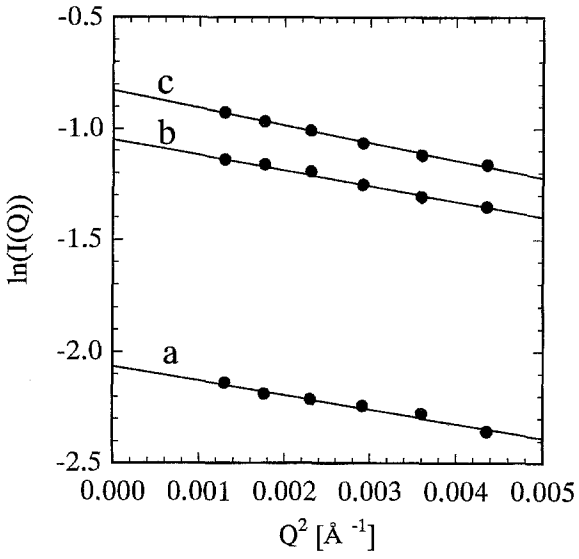

Fig. 5 $\ln I(Q)$ against Q^2 plots for the 2.0 wt% Ba(EOP)-D_2O solution at different temperatures (a: 23° C, b: 40° C, c: 50° C)

system. It is evident that the $I(Q)$ values for the 1.0 wt% solution arises from the monomers in solution, and that the neutron scattered intensities obtained at the higher concentration contain contributions from both monomers and micelles. The peak arising from the intermicellar interactions disappears in the intensity spectrum, indicating that the micellar concentration is very low and the intermicellar interaction can be neglected in region I. Therefore, the interparticle structure factor is reduced to unity.

Figure 4B shows the $I(Q)$ vs. Q plots for the 2.0 wt% sample solution at different temperatures. In these spectra, the scattered intensities arising from the monomers were subtracted from the observed intensities. Therefore, the scattered intensities, shown in Fig. 4B, pertain only to the micelles. As shown in Fig. 5, within the temperature range studied a Guinier plot ($\ln[I(Q)]$ vs. Q^2) provides a straight line in the small Q region, indicating that the intermicellar interaction can be neglected. Table 1 lists the R_g values of the 2.0 wt% sample at different temperatures. The Guinier radius tends to increase with an increase in temperature, indicating a temperature dependence of micellar size.

The shape and size of an Ba(EOP) micelle have been determined on the basis of the radius of gyration obtained from the Guinier plot. For the Ba(EOP) micellar model, we have assumed that a micelle consists of a hydrophobic core and a hydrophilic layer having a thickness equal to the diameter (4.2 Å) of the PO_4^- group. SANS intensity profiles for oblate spheroid, cylinder-like and disk-like models were also tested. However, the prolate spheroid model provided the best fit. For the minor axis (**b**) of the hydrophobic core, the assumed values of **b** were equal to the length (11.6 Å) of the all-*trans* *n*-octyl chain and 0.81 times ($\mathbf{b} = 0.81 \times 11.6$ Å) that for the extended *n*-octyl chains (obtained from the Tanford's equation [32]). Calculations have been made to provide the best fit between the radius of gyration obtained from the Guinier plots and theoretically-calculated results, as shown in Fig. 4B. The calculated intensity profile for the prolate spherical micelle having a minor axis $\mathbf{b} = 11.6$ Å has provided the best fit between the observed data points and the calculated results. Thus, for the micelles of Ba(EOP) in water, we have found that the shape is prolate and the **a**/**b** ratio depends on temperature. The aggregation number (**n**) tends to increase with an increase of temperature. The results are summarized in Table 1.

Micellar structure of Li(EOP)

Figure 6A shows the neutron scattering intensity spectra of the Li(EOP)-D_2O samples in region I. In these spectra, the scattered intensities arising from the monomers were subtracted from the observed intensities. Very broad peaks are seen in the SANS spectra within the concentration range 4 ~ 10 wt%, indicating the presence of intermicellar interactions in this system. The interaction peak increases steadily in intensity, and shifts to higher Q values as the concentration increases. Therefore, it seems that interactions between micellar particles are enhanced with increasing in concentration.

We may assume that a structural model of the Li(EOP) micelle is similar to that of the Ba(EOP) micelle. For the SANS analysis, prolate spheroid, oblate spheroid, cylinder-like and disk-like have been used as models of the shape, assuming mono-dispersity of micelles. We have found that the prolate-spheroid model provides the best fit to the observed data, as shown in Fig. 6A. The results are summarized in Table 2, together with the fitting parameters (**n** and α) and average percentage deviation per data point was $\pm 4\%$ for all spectra.

As is seen in Table 2, it is evident that the average aggregation number (**n**) increases with an increase in concentration. A ladder model of micellar growth [5], which has been successfully applied to SANS studies of micellar systems in many investigations [15, 17, 33–35], may be applied to the formation of the micelle in this system. Figure 7 shows the **n** as a function of the square root of the monomer concentration (molar fraction) forming the micelle in region I. All the **n** values fall on a straight line, thus suggesting a ladder model. Moreover, it can be seen that an **a**/**b** ratio of the prolate spheroidal micelle decreases as the concentration approaches the CMC. The result indicates that the micellar shape varies with an increase in micellar concentration. Extrapolation of the linear

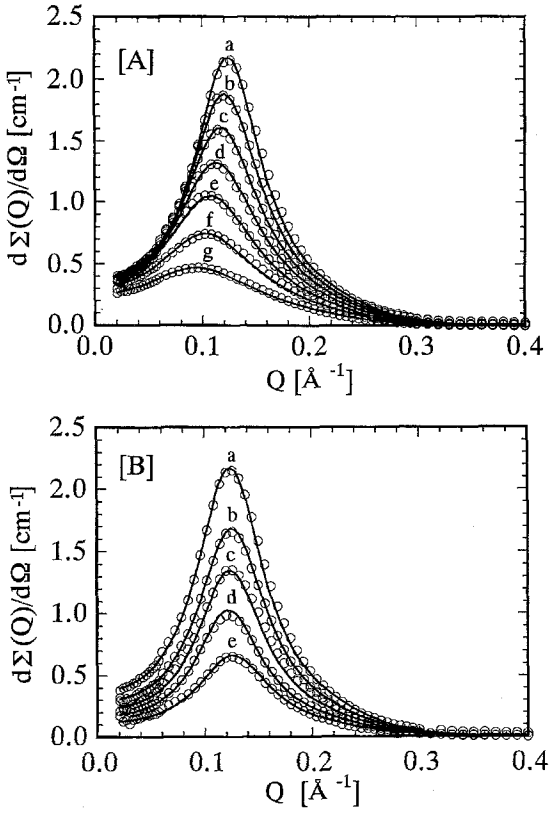

Fig. 6A Observed scattering intensity spectra (○) for the Li(EOP)-D_2O system at 23° C: a 10 wt%, b 9 wt%, c 8 wt%, d 7 wt%, e 6 wt%, f 5 wt% and g 4 wt%, and fitted scattering intensity profiles (solid lines) in the Q range 0.06 ~ 0.40 [Å^{-1}]. **B** Observed scattering intensity spectra (○) for the 10 wt% Li(EOP) solution at various D_2O% in the solvent: a 100% D_2O, b 90% D_2O, c 80% D_2O, d 70% D_2O and e 60% D_2O, and fitted scattering intensity profiles (solid lines) in the Q range 0.06 ~ 0.40 [Å^{-1}], assuming that the micelles are mono-dispersed

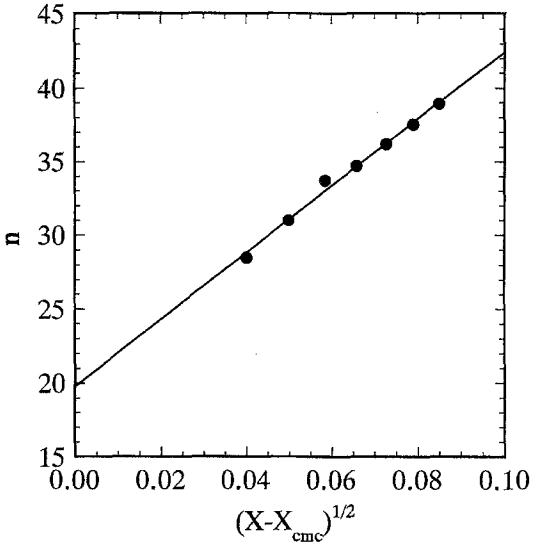

Fig. 7 A plot of **n** as a function of the square root of monomer concentration-forming-micelles

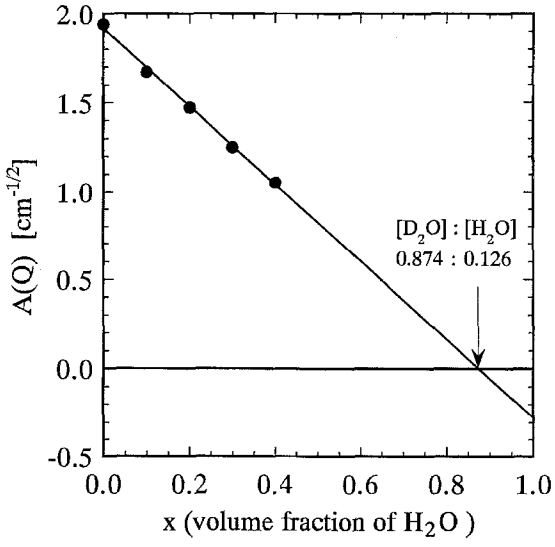

Fig. 8 External contrast variation plots for the 10 wt% Li(EOP) solution

$(X - X_{CMC})^{1/2}$ vs **n** plots provides the minimum aggregation number (**n** = 21) of a micelle at the CMC. For a micelle having the minimum aggregation number **n** = 21, an **a**/**b** ratio is 1.1, indicating that the minimum micelle may be spherical. Accordingly, for region I we may assume that both the micellar growth and the sphere to prolate shape variation occur with an increase in micellar concentration.

The SANS intensity spectra for the Li(EOP) 10 wt% solution at different $[D_2O]$:$[H_2O]$ ratios have also been measured, and are shown in Fig. 6B. For the observed intensity spectra, contrast variation analysis has been made using the Q-dependent quantity $A(Q)$ given by Sheu et al. [34].

$$A(Q) = [(d\Sigma(Q)/d\Omega)/P(Q)/S'(Q)]^{1/2} \quad (16)$$

$A(Q)$ can be calculated from the observed SANS spectra and substitution of the theoretical calculations of $P(Q)$ and $S'(Q)$. Since $A(Q)$ is linearly proportional to the scattering length density of the D_2O-H_2O mixed solvents, the contrast matching point, where the scattering intensity vanishes, can be determined by extrapolating the $A(Q)$ vs. x (volume fraction of H_2O) curve to zero. Figure 6B also shows the fitted curves of the scattering intensity vs Q plots at various $[D_2O]$:$[H_2O]$ ratios. Agreement between the observed intensities and the calculated results is excellent for all samples. The contrast variation plot is shown in Fig. 8. We have found that the contrast matching point occurs at a ratio of $[D_2O]$:$[H_2O]$ = 0.874: 0.126. The

Colloid & Polymer Science, Vol. 274, No. 3 (1996)

mean aggregation number (**n**) and volume value (V_{mol}) of an EOP molecule obtained from the slope and matching point are 37.3 and 352 Å^3, respectively.

The contrast matching point has been calculated, taking into account the mean value ($\alpha = 0.41$) for the degree of ionization, and has been found to occur at a ratio of $[D_2O]:[H_2O] = 0.876:0.124$. The calculated and observed matching point values are almost identical.

Conclusion

Mixed-double chain anionic surfactant molecules, barium- and lithium-salts of ethyl(*n*-octyl) phosphate (EOP), have been synthesized. The microstructure of aggregates in the EOP-water binary systems has been studied by SANS spectra.

For the micellar solution of EOP-barium salts in D_2O, it has been found by SANS analysis that the micellar shape is a prolate spheroid and that the aggregation numbers (**n**) are $\mathbf{n} = 48$ at 23° C and $\mathbf{n} = 52$ at 50° C.

For the micellar solution of EOP-lithium salts in water, SANS spectra have been measured and intensity profile calculations have been made. Calculations of the SANS data on the Li(EOP) system suggested a sphere to prolate transition due to a slight micellar growth.

Acknowledgment We express gratitude to Prof. Chairman J. O'Conner (University of Auckland, Department of Chemistry, New Zealand) for making suggestions for revision of the manuscript.

References

1. Israelachvili J (1992) Intermolecular & Surface Forces, Chap 16–17 Academic Press
2. Puvvada S, Blanckstein D (1990) J Chem Phys 92:3710–3724
3. Kato T, Seimiya T (1986) J Phys Chem 90:3159–3167
4. Herrington TM, Sahi SS (1988) J Colloid Interface Sci 21:107–120
5. Missel PJ, Mazer NA, Benedek GB, Young CY, Carey MC (1980) J Phys Chem 84:1044–1057
6. Malliaris A, Moigne J Le, Sturm J, Zana R (1985) J Phys Chem 89:2709–2713
7. Carnie SL, Israelachvili JN, Pailthorpe BA (1979) Biochim Biophys Acta 554:340–357
8. Hirata H, Taga K, Yoshida T, Okabayashi H (1993) Abstract for Symposium on Colloid and Surface Chemistry in Japan (Tokyo) 424–425
9. Yoshida T, Miyagai K, Taga K, Okabayashi H (1990) Magn Reson Chem 28:715–721
10. Yoshida T, Miyagai K, Aoki S, Taga K, Okabayashi H (1991) Colloid Polym Sci 269:713–719
11. Persson B-O, Drakenberg T, Lindman B (1979) J Phys Chem 83:3011–3015
12. Stilbs P, Lindman B (1984) J Colloid Interface Sci 99:290–293
13. Miyagai K, Taga K, Yoshida T, Okabayashi H, Nishio E (1991) Colloid Polym Sci 269:153–160
14. Berr SS, Caponetti E, Jhonson JS Jr, Jones RRM, Magid L (1986) J Phys Chem 90:5766–5770
15. Berr SS, Coleman MJ, Jones RRM, Johnson JS Jr (1986) J Phys Chem 90:6492–6499
16. Berr SS (1987) J Phys Chem 91: 4760–4765
17. Berr SS, Jones RRM (1989) J Phys Chem 93:2555–2558
18. McCombie H, Saunders BC, Stacey GJ (1945) J Chem Soc 380–382
19. Mukaiyama T, Fujisawa T (1961) Bull Chem Soc Jpn 34:812–813
20. Ishikawa Y, Furusaka M, Niimura N, Arai M, Hasegawa K (1986) J Appl Cryst 19:229–242
21. Furusaka M, Suzuya K, Watanabe N, Osawa M, Fujikawa I, Satoh S (1992) KENS REPORT-IX 25–27
22. Saers F (1987) Methods of Experimental Physics Vol 23, PART A 521–550 Academic Press
23. Suzuya K (1992) Ph D thesis, Tohoku University
24. Guinier A, Fournet G (1955) Small Angle Scattering of X-Rays; Wiley: New York
25. Lin TL, Chen SH, Gabriel NE, Roberts MF (1986) J Am Chem Soc 108: 3499–3507
26. Hayter JB, Penfold J (1981) J Mol Phys 42:109–118
27. Hayter JB, Penfold J (1981) J Chem Soc Faraday Trans I 77:1851–1863
28. Hansen JP, Hayter JB (1982) J Mol Phys 46:651–656
29. Wennerstrom H, Lindman B, Söderman O, Drakenberg T, Rosenholm J B (1979) J Amer Chem Soc 101:6860–6864
30. Vass S, Török T, Jákli G, Berecz E (1989) J Phys Chem 93:6553–6559
31. Marcus YJ (1983) J Solution Chem 12:271–275
32. Tanford C (1974) J Phys Chem 78: 2469–2479
33. Lin TL, Chen SH, Huang JS (1987) J Phys Chem 91:401–413
34. Sheu EY, Chen SH, Huang JS (1987) J Phys Chem 91:3306–3310
35. Lin TL, Tseng MY, Chen SH, Roberts MF (1990) J Phys Chem 94: 7239–7243